PCCP

Accepted Manuscript

ROYAL SOCIETY OF CHEMISTRY

www.rsc.org/pccp

Fe- and Co-P_4-embedded graphenes as electrocatalysts for the oxygen reduction reaction: theoretical insights

Liyan Feng,[a] Yuejie Liu,[b,*] Jingxiang Zhao,[a,*]

[a] College of Chemistry and Chemical Engineering, Harbin Normal University, Harbin 150025, China

[b] Modern Lab Center, Harbin Normal University, Harbin 150025, China

* To whom correspondence should be addressed. Email: xjz_hmily@163.com (JX); zhaojx1103@hotmail.com (YJ)

Abstract: Encouraged by the great promise of metal-nitrogen-carbon (M-N-C) materials in replacing Pt for catalyzing the oxygen reduction reaction (ORR), the metal-P species was successfully introduced into carbon matrix in experiment and exhibited high catalytic activity for the ORR. Here, by means of comprehensive density functional theory (DFT) computations, we investigated the origin and the mechanism of the occurring ORR on Fe- and Co-P-embedded graphenes. Our computations revealed that the Fe- and Co-P_4 moieties embedded graphenes possess good stability and high chemical reactivity for O_2 activation, thus facilitating the subsequent the ORR steps, and a more efficient 4e pathway in both acidic and alkaline media is more energetically favorable. Furthermore, by analyzing the computed free energy profiles, the Fe-P_4 species embedded graphene is more efficient electrocatalyst for the ORR in alkaline medium than the embedded Co-P_4 species into graphene. Our computations DFTs would be useful to gain deeper insight into the high activity of metal-P species.

Keywords: metal-P species; graphene; ORR; DFT computations

1. Introduction

As one of the most efficient electrochemical energy conversion devices, fuel cells, which can convert the chemical energy to electrical energy via electrochemical reactions, have achieved paramount interest in the past few decades due to their high conversion efficiency, high power density, and no pollution.[1-3] The oxygen reduction reaction (ORR) plays pivotal roles in fuel cells, which could greatly affect the chemical–electrical energy conversion efficiency. Nevertheless, the sluggish kinetics of the ORR has imposed great limitation for the better performance of fuel cells. To date, platinum (Pt)–based materials are still the most commonly employed electrocatalysts for ORR due to its high catalytic activity to reduce oxygen efficiently at low temperatures (normally 60~120 C°).[4] Although Pt–based catalysts are the best electrocatalyts identified theoretically, the scarcity, high cost, poor durability, and large overpotential of the Pt catalysts hinders the commercial applications of fuel cells. Therefore, the development of inexpensive and highly effective non-precious-metal or metal-free electrocatalysts has recently become a major focus in fuel cells.[5-14]

Ternary Fe/N/C is generally considered as one of the most promising candidates for replacing Pt for catalyzing ORR in fuel cells [15-21], which can be traced back to the pioneering work of transition-metal macrocyclic compounds by Jasinski.[22] For example, Zelenay et al. demonstrated that FeN_x embedded polymer materials exhibit high oxygen reduction activity, along with good performance durability.[23] Chen *et al.* synthesized Fe incorporated N-doped graphene which displays significantly enhanced electrocatalytic performance for ORR.[24] On the other hand, theoretical studies found

that the metal atom in such catalyst is the active center in the heterogeneous environment because it can form strong back bonding with the adsorbed O_2, which elongates the O-O bond distance and hence facilitates the ORR.[25-33] Especially, this Fe–N_x-embedded graphene catalyst features a more efficient 4e transfer process toward ORR in both acidic and alkaline media.[29]

Very recently, a new class of Fe-P species is demonstrated to possess high electrocatalytic activity for ORR in both acidic and alkaline media when it is incorporated in carbon matrix.[34, 35] In light of the effectiveness of Fe-P-C species for catalyzing ORR and the wide applications of graphene in the development of electrocatalysts, several questions arise: (i) Can the Fe-P system embedded into graphene be used as an electrocatalyst for ORR? (2) If yes, what is the mechanism for ORR on Fe-P center embedded graphene? (3) Since Co-N_x/C electrocatalysts exhibit high catalytic activity for the ORR,[33] can Co-P systems possess catalytic activity for ORR after embedding into graphene? To answer the above questions, in this work, we investigated the potential of Fe- and Co-P_4 incorporated graphenes as the electrocatalysts for the ORR in acidic and alkaline media by carrying out comprehensive DFT computations. Our DFT results suggest that the incorporated Fe-P_4 moiety into graphene exhibits excellent ORR catalytic activity under alkaline environments.

2. Computational methods and models

The spin–polarized DFT computations employed an all–electron method within a

generalized gradient approximation (GGA) for the exchange–correlation term, which was implemented in DMol^3 code.[36, 37] The double numerical plus polarization (DNP) basis set and PBE functional were adopted.[38] The accuracy of DNP basis set is comparable to that of Pople's 6–31G** basis set and exhibits excellent consistency with experiments.[39, 40] Especially, to accurately describe the long-range electrostatic interactions of ORR species with catalysts, the PBE+D2 method with the Grimme vdW correction was employed.[41] Self–consistent field (SCF) calculations were performed with a convergence criterion of 10^{-6} a.u. on the total energy and electronic computations. To ensure high quality results, the real-space global orbital cutoff radius was chosen as high as 4.7 Å in all the computations. A conductor-like screening model (COSMO) [42] was used to simulate a H_2O solvent environment throughout the whole process. The dielectric constant was set as 78.54 for H_2O solvent. All data were obtained under this method unless mentioned otherwise.

We set the *x* and *y* directions parallel and the *z* direction perpendicular to the plane of these graphene-based systems, and adopted a supercell length of 15 Å in the *z* direction. A 5 × 5 supercell consisting of 50 carbon atoms containing 50 atoms was constructed. Graphitic metal-P_4 defects were created by substituted the four carbon atoms around graphene double vacancy (DV) with four phosphorus atoms, and then incorporating metal atom at the center of DV. The Brillouin zone was sampled with a 5 × 5 × 1 *k* points setting in geometry optimizations, and a 12 × 12 × 1 grid was used for electronic structure computations. The transition states were located by using the synchronous method with conjugated gradient refinements. This method involves

linear synchronous transit (LST) maximization, followed by repeated conjugated gradient (CG) minimizations, and then quadratic synchronous transit (QST) maximizations and repeated CG minimizations until a transition state is located.[43] In order to ascertain the reliability of computations in 5 × 5 supercells, we repeated related computations for graphene in 6 × 6 supercells, and detailed results are shown in Table S1 in the Supporting Information. Small differences between the results of 5 × 5 and 6 × 6 supercells guarantee the validity of the conclusions in this work.

The adsorption energy (E_{ad}) was defined as $E_{ad} = E_{adsorbate/substrate} - E_{adsorbate} - E_{substrate}$, where $E_{adsorbate/substrate}$, $E_{adsorbate}$, $E_{substrate}$ are the total energies of the adsorbed systems, the free adsorbate, and the substrate, respectively. With this definition, a negative value indicates an exothermic adsorption. The charge transfer was calculated according to Hirshfeld method.[44] The change in free energy (ΔG) of a reaction step on the M-P_4/graphenes was calculated based on a computational hydrogen electrode (CHE) model suggested by Nøskov et al.[45-47] In detail, free energy change was determined by $\Delta G = \Delta E + \Delta E_{ZPE} - T\Delta S + \Delta G_{pH} + \Delta G_U$, where ΔE is the reaction energy directly obtained from DFT calculations, E_{ZPE} is the zero–point energies, T is temperature (298.15 K), and ΔS is the change in entropy. $\Delta G_U = -neU$, where n is the number of electrons transferred and U is the electrode potential. ΔG_{pH} is the correction of the H^+ free energy by the concentration $\Delta G_{pH} = k_B T \times \ln 10 \times pH$, where k_B is the Boltzmann constant and pH = 0 and 14 in acidic and alkaline conditions. Zero–point energies and entropies of the ORR intermediates were calculated from the vibration frequencies. The entropies and vibrational frequencies of molecules in the

gas–phase are taken from the NIST database,[45] while the vibrational frequencies of adsorbed species were calculated to obtain ZPE contribution in the free energy expression. Only adsorbate vibrational modes were calculated explicitly, while the functionalized graphene sheets are fixed (assuming vibrations of the embedded graphene sheets are negligible) as done in previous theoretical studies.[47-51]

3. Results and Discussion

3.1. Stability of M–P_4 embedded graphene.

Firstly, we optimized the P_4 structure embedded in a 5×5 graphene supercell. Our computations revealed that a rectangle-like P_4 configuration is obtained with the P-P bond lengths of 2.34 and 2.73 Å, respectively (Figure 1a). The P-C bond length is about 1.76 Å, which is much larger than 1.42 Å for C-C sp^2 bonds. The 24% increase in the bond length forces the four P atoms protrude from the graphene plane by ~1.50 Å, also displacing the positions of the nearest C atoms out of the plane in various ways. Then, we place the Fe and Co above the center of the P_4 structure embedded graphene. After geometrical optimization, four equivalent Fe–P or Co–P bonds are formed with the distance of 2.09 (Figure 1b) and 2.07 Å (Figure 1c). Due to the large size of metal atom as compared with P atom, the adsorbed Fe and Co atoms moves outward the basal plane of P_4 structure by about 0.65 and 0.55 Å, respectively.

Aiming to evaluate the stability of M–P_4 embedded graphene sheet, which is a key challenge in fabrication of practical and stable single–atom catalysts, the binding strength of Fe and Co atoms at P_4–configuration embedded graphene sheet is thus

computed. The results indicated that binding energies of Fe and Co on the P_4–configuration are -6.34 and -6.54 eV, which is higher than the cohesive energies of the corresponding metals,[52] implying the high stability of Fe– and Co–P_4 species. The diffusion of Fe on graphene from the P_4 site to its neighboring H–site is endothermic by 5.15 eV and the computed energy barrier is 6.04 eV, which vigorously excludes the clustering problem. The strong interaction of Fe or Co with P_4–configuration embedded graphene sheet is mainly attributed to the geometry distortion of the P_4 moiety upon Fe or Co atom. To test this hypothesis, Fe or Co adsorption energy on the embedded P_4 configuration inside graphene was recalculated by freezing the positions of the atoms in the P_4/graphene system. The calculated adsorption energies of Fe and Co on the frozen P_4/graphene substrate are -5.04 and -5.05 eV, respectively, which are smaller than those of on the fully relaxed P_4/graphene substrate (-6.34 and -6.54 eV). Clearly, the deformation energies make a great contribution to the high adsorption energy of Fe and Co on P_4/graphene substrate.

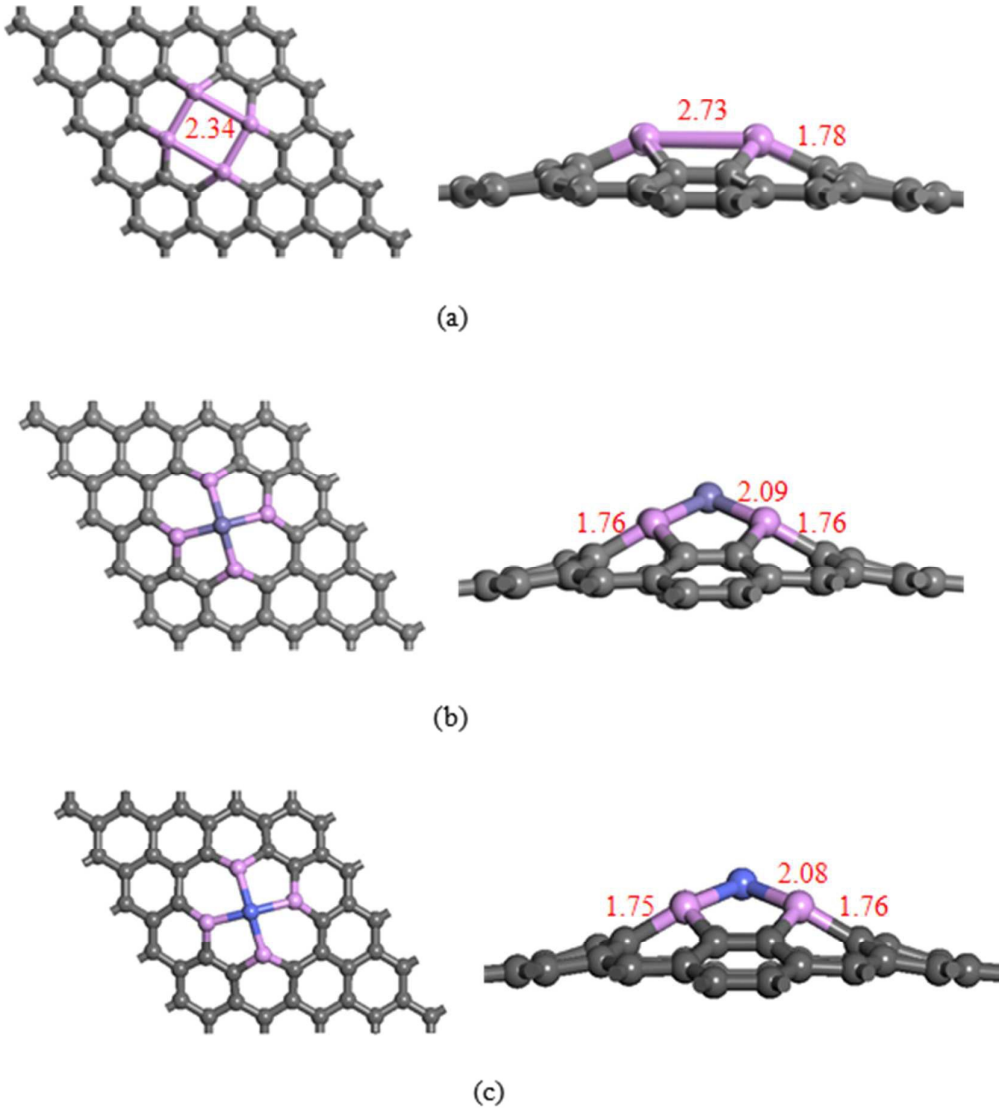

Figure 1. The top and side views of the optimized geometrical structures of (a) P_4, (b) Fe-P_4, and (c) Co-P_4 embedded graphene. The unit of bond length is Å.

Another important question is that the center metal atom of the metal atoms embedded graphene could be corroded under acidic environment, leading to their poor long-term stability, in which the metal atoms could be replaced by two protons and this substitution reaction can be written as: M-P_4/graphene + $2H^+$ = 2H-P_4/graphene + M^{2+}. To examine the stability of the proposed catalysts, we thus computed the free

energy change caused by substituting one Fe or Co atom with two protons. The computed Gibbs energies for Fe- and Co-P_4 embedded graphene were 1.59 and 1.51 eV, respectively, demonstrating that the substitution reactions are rather difficult to occur. With increasing electrode potential and pH, the substitution of Fe or Co atom by two protons would be more and more endothermic for the two catalysts. Thus, Fe- and Co-P_4 in the embedded graphene is resistant to dissociation, ensuring their stability against corrosive acidic and alkaline media.

3.2. O_2 adsorption on M-P_4 embedded graphene.

Generally, the favorable adsorption of O_2 is a prerequisite for ORR to proceed on the surface of catalyst. To obtain the most stable configuration for O_2 adsorption, we constructed various starting geometries, including end-on configuration and the side-on configuration, by placing O_2 in different nonequivalent positions of M-P_4 embedded graphene monolayer.

After geometrical optimization, we found that the side-on configurations is the most energetically favorable on the two catalysts (Figure 2a and b), and the O_2 adsorption energies was −1.03 and −0.85 eV on Fe- and Co-P_4 embedded graphene. The distance of the newly formed metal-O bond is 1.92 Å. Because there is about 0.22 and 0.18 |e| charge transfer from Fe- and Co-P_4 embedded graphene to O_2, which could occupy the antibonding $2\pi^*$ orbitals of O_2, the O-O bond is elongated from 1.21 Å of the free O_2 to 1.37 Å of the adsorbed O_2, a typical value of peroxo species.

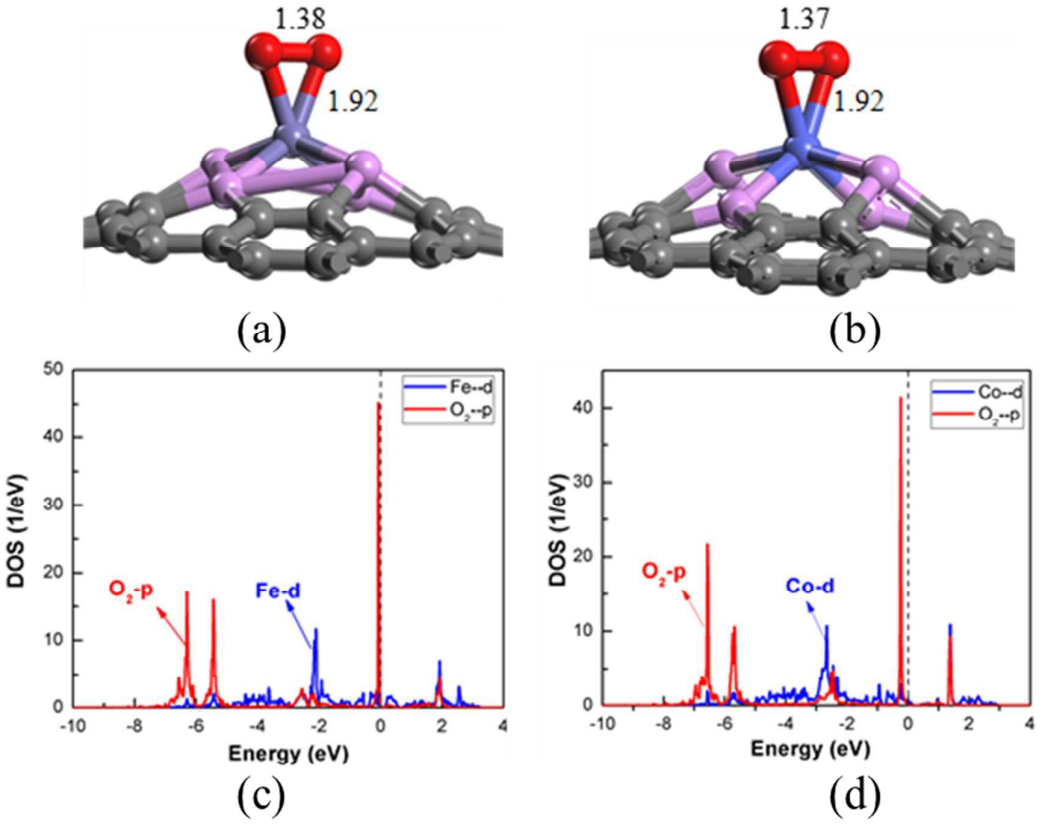

Figure 2. The optimized structures of O_2 on (a) Fe- and (b) Co-P_4 embedded graphene, and the (c) and (d) corresponding projected density of states.

To get a deeper understanding on the mechanism of O_2 activation on Fe- and Co-P_4 embedded graphene, we computed the partial density of states for O_2 adsorbed the two catalysts. Our DFT computations revealed that there is an obvious hybridization between the O_2-2*p* orbitals and Fe- and Co-3*d* orbitals (Figure 2c and d). Thus, the above results demonstrated that O_2 molecule can be sufficiently activated on Fe- and Co-P_4 embedded graphenes, which would facilitate its subsequent reduction reactions.

The next important question is whether the chemisorbed O_2 molecule on Fe- and

Co-P_4 embedded graphene surfaces undergoes the O-O bond dissociation to form two separated O atoms. To address this question, we examine the O_2 dissociation pathway on the two catalysts. At the final state, one O atom is adsorbed on the top of metal atom and the other O atom is adsorbed between two neighboring P atoms to form a three–membered ring (Figure S1 in Supporting Information). Furthermore, the activation barrier of O_2 dissociation on Fe- and Co-P_4 center is 1.21 and 1.02 eV, suggesting that this process is unlike to proceed at working temperature, which is similar to that of on the Fe-Pc monolayer because they possess similar active sites for the adsorption of dissociated O atoms.[53]

In addition, we also examine the adsorption of other ORR species, including OOH, O, OH, HOOH, and H_2O on Fe– and Co–P_4 embedded graphene (Figure S2). Our computations showed that all of the ORR species would bind favorably to the central transition metal Fe or Co atom with the adsorption energies ranging from -0.40 to -4.40 eV (Table 1). We note that the OOH, OH, and O can bind strongly with Fe– and Co–P_4 embedded graphene with the larger adsorption energy, whereas the interaction of H_2O and the two catalysts is comparatively weak, making it easily release from the catalysts once it is formed. For HOOH species, we find that it is unlike to maintain its chemical structure on the Fe–P_4 center and would spontaneously decomposes into O + H_2O species after structural optimization (Figure S2g). The calculated adsorption energy is -2.53 eV (Table 1) and the shortest distance between the dissociated HOOH and Fe–P_4 center is 1.69 Å. In contrast, the adsorption behavior of the HOOH species on the Co–P_4 complex is completely different, where

the HOOH species remains structurally intact (Figure S2h), corresponding to a small adsorption energy of -0.47 eV (Table 1) and a long distance between each other (2.08 Å).

3.3. ORR on M-P_4 systems in acid medium.

After obtaining the stable configuration of various ORR species on the two catalysts, we further investigated the elementary ORR steps on the surface of Fe- and Co-P_4 center embedded graphene both in acid and alkaline media.

The complete 4e^- ORR in acidic medium proceeds *via* the following reactions [54]:

$$O_2 + 4(H^+ + e^-) \rightarrow {}^*O_2 + 4(H^+ + e^-) \quad (1)$$

$${}^*O_2 + 4(H^+ + e^-) \rightarrow {}^*OOH + 3(H^+ + e^-) \quad (2)$$

$${}^*OOH + 3(H^+ + e^-) \rightarrow {}^*O + H_2O + 2(H^+ + e^-) \quad (3)$$

$${}^*O + H_2O + 2(H^+ + e^-) \rightarrow {}^*OH + (H^+ + e^-) \quad (4)$$

$${}^*OH + H_2O + H^+ + e^- \rightarrow 2H_2O \quad (5)$$

Alternatively, H_2O_2 can form instead of the product in eqn (2) and desorb from the catalytic site as a stable intermediate and the left superscript "*" stands for an active site on the Fe– and Co–P_4 embedded graphene. In Figure 3, we presented the stationary points of the ORR and the corresponding free energies and energy barriers on Fe– and Co–P_4 embedded graphenes.

Our DFT computations revealed that the activated O_2 molecule can be easily hydrogenated with the help of H and form an OOH group adsorbed on Fe or Co site. In this configuration, the bond between the Fe or Co atom and the adsorbed O atom

by H atom are elongated to 2.78 and 2.45 Å, while the other Fe- or Co-O bond length is shortened to 1.83 and 1.87 Å. Meanwhile, the O-O bond is further elongated to 1.46 Å. Notably, the above step is exothermic in the free energy profile by 0.58 and 0.50 eV on Fe-P_4 and Co-P_4 complex (Figure 3) and the computed energy barrier is 0.53 and 0.57 eV. For the formed OOH species, it cannot directly dissociate into O + OH on the two catalysts at working temperature owing to the large barrier of 0.91 and 1.02 eV.

Subsequently, we introduced the second H to the two systems to examine the hydrogenation of the formed OOH^* species. Because of random nature, this H atom can be adsorbed on both O sites. Hence, the ORR can further proceed following two different pathways, one is the four-electron (4e) reduction pathway in which O_2 is reduced to two H_2O molecules, and the other is the two-electron (2e) reduction pathway in which O_2 is reduced to a H_2O_2 molecule.

In the 4e reduction pathway, the first H_2O molecule would be created after the adsorption of H on the pre-hydrogenated O site of OOH group. This process is downhill in the free energy profile by 2.03 and 1.65 eV on Fe- and Co-P_4 center (Figure 3). This step also has a moderate free energy barrier of 0.42 and 0.56 eV. In the transition state, the O-O bond is stretched to 1.53 Å, indicating that the OH group starts to leave OOH* and form chemical bonding with H. After the release of H_2O, the remaining O atom is locating on the Fe and Co atoms with the Fe- and Co-O length of 1.67 and 1.72 Å, which can react with another proton to yield an OH group, which is still adsorbed at the Fe and Co sites and has a Fe- and Co-O bond of 1.85 and 1.88 Å.

In the two hydrogenation processes, the Gibbs free energies decrease by 1.12 and 1.55 eV, along with the energy barriers of 0.24 and 0.37 eV. Finally, the adsorbed OH group reacts with one proton upon one-electron reduction to form another H_2O molecule (Figure 3). This final step is also downhill in the free energy profile by 0.89 and 1.01 eV. Especially, the formed H_2O molecule can be effectively removed from the surface in terms of its weak binding strength with Fe- and Co-P_4 complex.

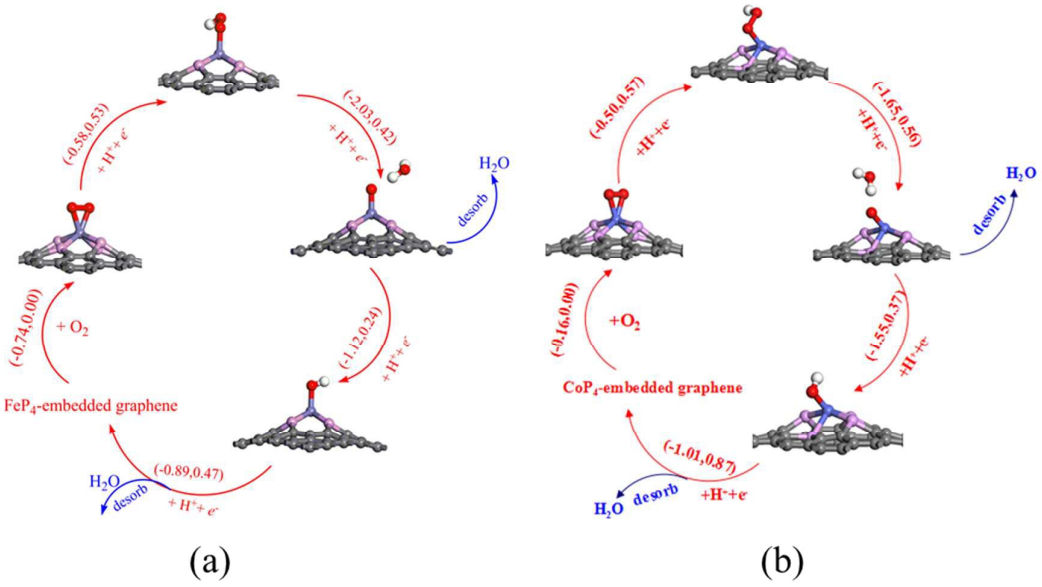

Figure 3. The whole ORR pathway on (a) FeP_4- and (b) CoP_4-embedded graphene and the corresponding changes of free energies and energy barriers.

For the 2e reduction pathway, the proton binds to the pre-unhydrogenated O site of OOH group to form a H_2O_2 molecule. Our DFT found that the HOOH species would spontaneously dissociate into O + H_2O on Fe-P_4 moiety (Figure Sx), indicating that the 2e reduction pathway is unfavorable on Fe-P_4 embedded graphene. On the contrary, the ΔG of this process, $OOH^* + H^+ + e^- \rightarrow HOOH$ on Co-P_4 complex is

−0.18 eV, which is much less favorable than that of OOH* reduction to O*+H_2O in the 4e reduction pathway (ΔG = −1.65 eV). As the computed adsorption energy of H_2O_2 molecule on Co-P_4 embedded graphene is −0.47 eV (corresponding to the positive ΔG of 0.16 eV), the formed H_2O_2 species easily escape from the surface of Co-P_4 embedded graphene into the solution, thus completing the 2e reduction.

In Figure 4, we plot the effects of potential on the free energies of the ORR on the two catalysts in acidic media. We found that all ORR steps on Fe- and Co-P_4 embedded graphene are downhill in the free energy profile at *zero* potential. However, with the increase of the potential, some of the intermediate steps turn to be uphill. In the case of the Fe-P_4 embedded graphene, the maximum value of potential at which all reactions are still exothermic (namely, limiting potential) is 0.42 V, while the same is 0.50 V in the case of the Co-P_4-based catalyst. Thus, that the Co-P_4 system is a slighter better candidate as the ORR catalyst in acid medium than Fe-P_4 system. Especially, the ORR on Fe-, and Co-P_4 embedded graphenes prefer the 4e reduction pathway rather than the 2e reduction pathway, which is a big advantage for Fe- or Co-P system as ORR catalysts because H_2O_2 is an undesirable ORR product which could significantly affect the durability of fuel cells.

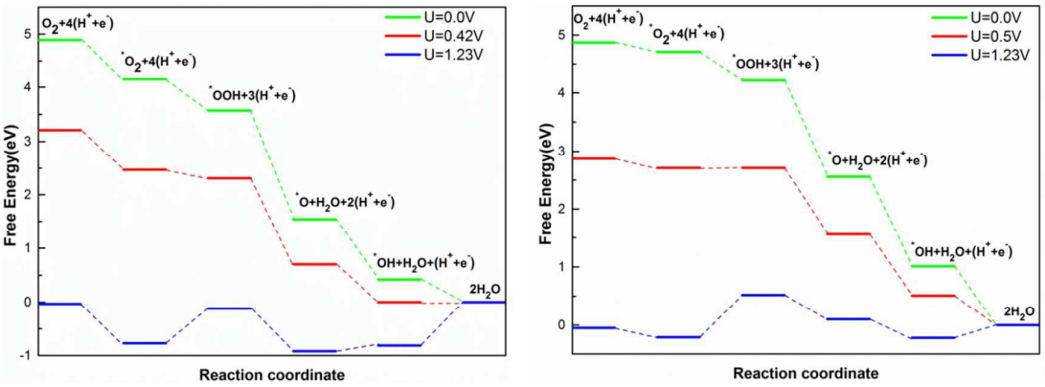

Figure 4. Free energy diagram for the ORR on (a) Fe- and (b) Co-P_4 embedded graphene in acid media.

3.4. ORR on M-P_4 systems in alkaline medium.

In alkaline medium, the complete 4e ORR takes place via the following reactions [54]:

$$O_2 + 2H_2O + 4e^- \rightarrow {}^*O_2 + 2H_2O + 4e^- \quad (6)$$

$${}^*O_2 + 2H_2O + 4e^- \rightarrow {}^*OOH + OH^- + H_2O + 3e^- \quad (7)$$

$${}^*OOH + OH^- + H_2O + 3e^- \rightarrow {}^*O + 2(OH^-) + H_2O + 2e^- \quad (8)$$

$${}^*O + 2(OH^-) + H_2O + 2e^- \rightarrow {}^*OH + 3(OH^-) + e^- \quad (9)$$

$${}^*OH + 3(OH^-) + e^- \rightarrow 4(OH^-) \quad (10)$$

The computed free energy profiles at different potentials in alkaline medium were presented in Figure 5. The results revealed that OOH formation is uphill for both the systems at *zero* potential. Moreover, the maximum value of potential at which all reactions turn to be downhill on Fe-P_4 system is 0.25 V, which is slightly smaller than that of on Co-P_4 system (0.33 V). Hence, in alkaline environments, Fe-P_4 moiety embedded graphene is more efficient catalyst for the ORR, as compared to Co-P_4

system. Furthermore, it can be seen that from the free energy diagrams both in acidic and alkaline media, at higher potentials, 0.33 V < U < 0.42 V, all elementary reaction steps of ORR are predicted to be downhill. In contrast, U > 0.42, an increasing number of uphill processes are found in acidic medium. In summary, O_2 reduction on Fe-P_4 species embedded graphene at higher potential is the most favorable, which is also observed in the case of graphitic metal-N_x.[33, 49]

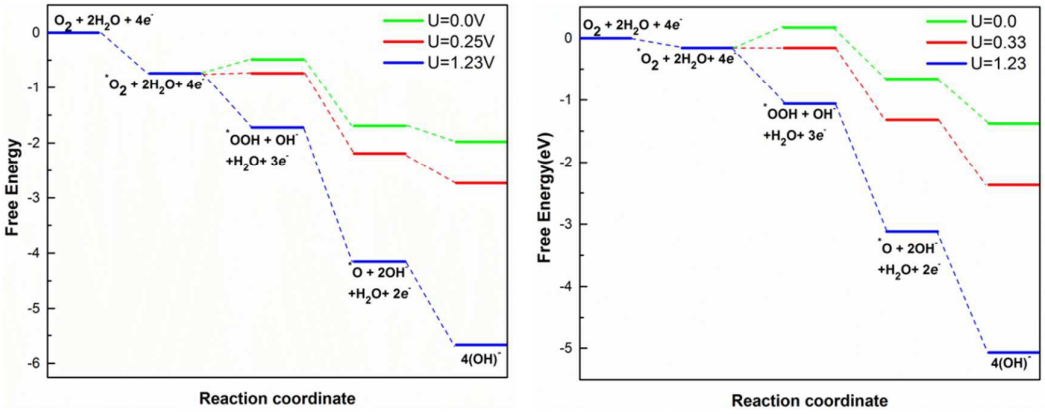

Figure 5. Free energy diagram for the ORR on (a) Fe- and (b) Co-P_4 embedded graphene in alkaline media.

Finally, using Fe-P system as a representative, we evaluated the potential of other Fe-P configurations embedded graphene as the electrocatalysts for the ORR, including Fe-P_1, Fe-P_2, and Fe-P_3 systems. Because the catalytic activity of an electrocatalyst for ORR is highly dependent on the adsorption energy of O_2 on catalyst surfaces, we utilized the calculated O_2 adsorption energy as a performance indicator of different Fe-P moieties embedded graphene for ORR. The computed most stable configurations of O_2 on the three Fe-P systems are presented in Figure S3. Our DFT results indicated

that the end–on configuration is the most energetically favorable for O_2 on Fe–P_1, Fe–P_2, and Fe-P_3 center with the adsorption energies of –2.22, –2.15 and -2.61 eV. Moreover, the O-O bond lengths are stretched by 0.18, 0.16 and 0.18 Å, as compared with the isolated O_2 (1.22 Å), which is ascribed to the charge transfer from the Fe-3*d* orbtials to the O_2-$2\pi^*$ orbitals (about 0.30 *e*). Thus, the adsorbed O_2 on these Fe-P systems are sufficient activated. According to the Sabatier principle,[55] however, an ideal catalyst should bind with the reaction species not too strongly nor too weakly. Although the adsorbed O_2 molecule on Fe-P_1, Fe-P_2 and Fe-P_3 systems is also be activated, the adsorption energy of O_2 to the catalyst is too large, suggesting that the three Fe-P moieties embedded graphene cannot be a good electrocatalyst for ORR. In addition, due to the elongated bonding length of M-P, there is a strain existed in the catalysts, which will have a great influence on its ORR performance. Hence, taking Fe-P_4/graphene system as an example, we investigated the strain effect on its catalytic activity for the ORR, in which the 5% strain was adopted. As shown in Figure S4, the calculated limiting potentials of the ORR on Fe-P_4/graphene are 0.14 V in acid media, which is smaller than that of no strain case (0.42 V). Moreover, in alkaline media, the limiting potential (0.69 V) under 5% strain is larger than that of no strain case (0.25 V). Therefore, we expected that the strain has a negative effect on the catalytic performance of the M-P moiety embedded in graphene in both acid and alkaline media.

4. Conclusions

In summary, our DFT computations show that the formation of Fe- and Co-P_4 moiety embedded into graphene is energetically favorable, which can effectively active the O_2 molecule, and promote the subsequent ORR to proceed via a more efficient 4*e* reduction mechanism in both acid and alkaline medium. On the basis of the plotted free energy profiles, the limiting potentials for ORR on Fe- and Co-P_4 centers are computed to be 0.42 and 0.50 V in acid medium, and 0.25 and 0.33 V in alkaline medium, indicating that the embedded Co-P_4 into graphene exhibit better performance for the ORR in acid media, whereas the Fe-P_4 species embedded graphene is a more efficient ORR catalyst in alkaline medium.

Acknowledgment. This work is supported by the National Natural Science Foundation of China (No. 21203048), the Scientific Research Fund of Heilongjiang Provincial Education Department (NO: 12531195), and the Excellent Young Foundation of Harbin Normal University (No. XKYQ201304). The authors would like to show great gratitude to the reviewers for raising invaluable comments and suggestions.

Supporting Information

The optimized structures of the products O_2 dissociation on Fe- and Co-P_4 embedded graphenes, various ORR species adsorption configurations on Fe- and Co-P_4 embedded graphenes, and O_2 adsorption on (a) Fe-P_2 and (b) Fe-P_3 embedded graphenes.

References

1. G. J. K. Acres, *J. Power Sources*, 2001, 100, 60-66.

2. E. Antolini, *J. Power Sources*, 2007, 170, 1-12.

3. C. Lamy, A. Lima, V. LeRhun, F. Delime, C. Coutanceau and J.-M. Léger, *J. Power Sources*, 2002, 105, 283-296.

4. M. Watanabe and H. Uchida, in *Fuel Cell Catalysis*, John Wiley & Sons, Inc., 2008, 10, 317-341.

5. Y. Nie, L. Li and Z. Wei, *Chem. Soc. Rev.*, 2015, 44, 2168-2201.

6. A. Morozan, B. Jousselme and S. Palacin, *Energy & Environ. Sci.*, 2011, 4, 1238-1254.

7. D. Banham, S. Ye, K. Pei, J.-i. Ozaki, T. Kishimoto and Y. Imashiro, *J. Power Sources*, 2015, 285, 334-348.

8. L. Dai, Y. Xue, L. Qu, H.-J. Choi and J.-B. Baek, *Chem. Rev.*, 2015, 115, 4823-4892.

9. X. Ge, A. Sumboja, D. Wuu, T. An, B. Li, F. W. T. Goh, T. S. A. Hor, Y. Zong and Z. Liu, *ACS Catal.*, 2015, 5, 4643-4667.

10. J. Duan, S. Chen, M. Jaroniec and S. Z. Qiao, *ACS Catal.*, 2015, 5, 5207-5234.

11. Y. Zheng, Y. Jiao and S. Z. Qiao, *Adv. Mater.*, 2015, DOI: 10.1002/adma.201500821.

12. M. E. Scofield, H. Liu and S. S. Wong, *Chem. Soc. Rev.*, 2015, 44, 5836-5860.

13. K. Chen, S. Song, F. Liu and D. Xue, *Chem. Soc. Rev.*, 2015, **44**, 6230-6257.

14. B. Xia, Y. Yan, X. Wang and X. W. Lou, *Mater. Hori.*, 2014, 1, 379-399.

15. J. Masa, W. Xia, M. Muhler and W. Schuhmann, *Angew. Chem. Int. Ed.*, 2015, 54, 10102–10120.

16. C. W. B. Bezerra, L. Zhang, K. Lee, H. Liu, A. L. B. Marques, E. P. Marques, H. Wang and J. Zhang, *Electrochim. Acta*, 2008, 53, 4937-4951.

17. Z. Chen, D. Higgins, A. Yu, L. Zhang and J. Zhang, *Energy & Environ. Sci*, 2011, 4, 3167-3192.

18. F. Jaouen, E. Proietti, M. Lefevre, R. Chenitz, J.-P. Dodelet, G. Wu, H. T. Chung, C. M. Johnston and P. Zelenay, *Energy & Environ. Sci*, 2011, 4, 114-130.

19. G. Wu and P. Zelenay, *Acc. Chem. Res.*, 2013, 46, 1878-1889.

20. J. H. Zagal, S. Griveau, J. F. Silva, T. Nyokong and F. Bedioui, *Coord. Chem. Rev.*, 2010, 254, 2755-2791.

21. J. H. Lee, M. J. Park, S. J. Yoo, J. H. Jang, H.-J. Kim, S. W. Nam, C. W. Yoon and J. Y. Kim, *Nanoscale*, 2015, 7, 10334-10339.

22. R. Jasinski, *Nature*, 1964, 201, 1212-1213.

23. R. Bashyam and P. Zelenay, *Nature*, 2006, 443, 63-66.

24. M. Chen, J. Liu, W. Zhou, J. Lin and Z. Shen, *Sci. Rep.*, 2015, 5.

25. S. Kattel and G. Wang, *J. Phys. Chem. Lett.*, 2014, 5, 452-456.

26. A. G. Saputro and H. Kasai, *Phem. Chem. Chem. Phys.*, 2015, 17, 3059-3071.

27. Z. Lu, G. Xu, C. He, T. Wang, L. Yang, Z. Yang and D. Ma, *Carbon*, 2015, 84, 500-508.

28. S. Stolbov and M. Alcántara Ortigoza, *J. Chem. Phys.*, 2015, 142, 154703.

29. W. Liang, J. Chen, Y. Liu and S. Chen, *ACS Catal.*, 2014, 4, 4170-4177.

30. S. Kattel, P. Atanassov and B. Kiefer, *Phem. Chem. Chem. Phys.*, 2014, 16, 13800-13806.

31. C. E. Szakacs, M. Lefevre, U. I. Kramm, J.-P. Dodelet and F. Vidal, *Phem. Chem. Chem. Phys.*, 2014, 16, 13654-13661.

32. S. Kattel and G. Wang, *J. Mater. Chem. A*, 2013, 1, 10790-10797.

33. S. Kattel, P. Atanassov and B. Kiefer, *Phem. Chem. Chem. Phys.*, 2013, 15, 148-153.

34. K. P. Singh, E. J. Bae and J.-S. Yu, *J. Am. Chem. Soc.*, 2015, 137, 3165-3168.

35. F. Razmjooei, K. P. Singh, E. J. Bae and J.-S. Yu, *J. Mater. Chem. A*, 2015, 3, 11031-11039.

36. B. Delley, *J. Chem. Phys.*, 1990, 92, 508-517.

37. B. Delley, *J. Chem. Phys.*, 2000, 113, 7756-7764.

38. J. P. Perdew, K. Burke and M. Ernzerhof, *Phys. Rev. Lett.*, 1996, 77, 3865-3868.

39. J. A. Rodriguez, S. Ma, P. Liu, J. Hrbek, J. Evans and M. Pérez, *Science*, 2007, 318, 1757-1760.

40. Z. Wu, L. Xu, W. Zhang, Y. Ma, Q. Yuan, Y. Jin, J. Yang and W. Huang, *J. Catal.*, 2013, 304, 112-122.

41. S. Grimme, *J. Comput. Chem.*, 2006, 27, 1787-1799.

42. A. Klamt and G. Schuurmann, *J. Chem. Soc., Perkin Transactions 2*, 1993, DOI: 10.1039/P29930000799, 799-805.

43. N. Govind, M. Petersen, G. Fitzgerald, D. King-Smith and J. Andzelm, *Comput.*

Mater. Sci., 2003, 28, 250-258.

44. F. L. Hirshfeld, *Theoret. Chim. Acta*, 1977, 44, 129-138.

45. J. K. Nørskov, J. Rossmeisl, A. Logadottir, L. Lindqvist, J. R. Kitchin, T. Bligaard and H. Jónsson, *J. Phys. Chem. B*, 2004, 108, 17886-17892.

46. J. Rossmeisl, A. Logadottir and J. K. Nørskov, *Chem. Phys.*, 2005, 319, 178-184.

47. A. A. Peterson, F. Abild-Pedersen, F. Studt, J. Rossmeisl and J. K. Norskov, *Energy & Environ. Sci.*, 2010, 3, 1311-1315.

48. D.-H. Lim and J. Wilcox, *J. Phys. Chem. C*, 2012, 116, 3653-3660.

49. S. Kattel, P. Atanassov and B. Kiefer, *J. Phys. Chem. C*, 2012, 116, 17378-17383.

50. Y. Wang, H. Yuan, Y. Li and Z. Chen, *Nanoscale*, 2015, DOI: 10.1039/C5NR00302D.

51. M. Li, L. Zhang, Q. Xu, J. Niu and Z. Xia, *J. Catal.*, 2014, 314, 66-72.

52. P. H. T. Philipsen and E. J. Baerends, *Phys. Rev. B*, 1996, 54, 5326-5333.

53. Y. Wang, H. Yuan, Y. Li and Z. Chen, *Nanoscale*, 2015, 7, 11633-11641.

54. Y. Jiao, Y. Zheng, M. Jaroniec and S. Z. Qiao, *Chem. Soc. Rev.*, 2015, 44, 2060-2086.

55. Y. Jiao, Y. Zheng, M. Jaroniec and S. Z. Qiao, *J. Am. Chem. Soc.*, 2014, 136, 4394-4403.

Table 1. The adsorption energies (E_{ads}, eV) and band lengths (d, Å) of various ORR species on Fe- and Co-P_4 embedded graphenes.

	Fe-P_4			**Co-P_4**		
	E_{ads}	$d_{Fe\text{-}O}$	$d_{O\text{-}O}$	E_{ads}	$d_{Co\text{-}O}$	$d_{O\text{-}O}$
O_2	-1.03	1.92	1.38	-0.85	1.92	1.37
OOH	-2.04	1.83	1.46	-1.51	1.87	1.46
OH	-3.19	1.85	/	-2.59	1.88	/
O	-4.40	1.67	/	-3.39	1.72	/
H_2O	-0.42	2.00	/	-0.40	2.13	/
H	-2.61	1.52(Fe-H)	/	-2.33	1.49(Co-H)	/
HOOH	-2.53	1.69	2.67	-0.47	2.08	1.50

The Table of Contents

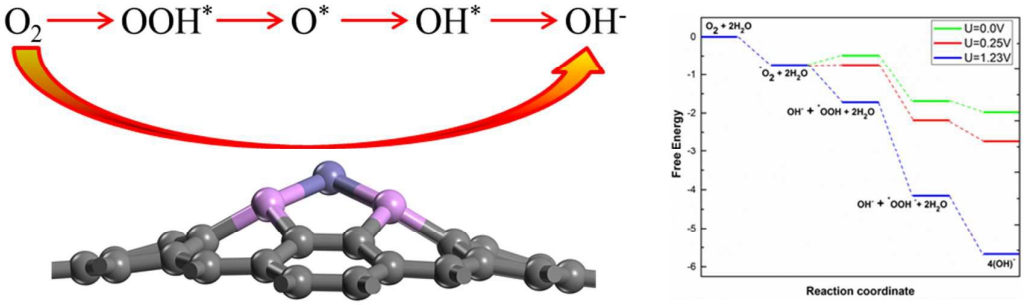

Fe-P_4-embedded graphene exhibits high catalytic activity for the ORR in alkaline media.